Acta Materialia (2010), 58 (8) 3014–3021
DOI: http://dx.doi.org/10.1016/j.actamat.2010.01.033

Microstructural characterization of alumina zirconia layered ceramics using positron annihilation spectroscopy

P. Parente [a,*], Y. Ortega [b], B. Savoini [a], M.A. Monge [a], A. Tucci [c], L. Esposito [c], A.J. Sánchez-Herencia [d]

[a] *Departamento de Física, Universidad Carlos III de Madrid, 28911 Leganés, Spain*
[b] *Departamento de Física de Materiales, Facultad de Ciencias Físicas, Univ. Complutense de Madrid, 28040 Madrid, Spain*
[c] *Centro Ceramico Bologna, 40128 Bologna, Italy*
[d] *Instituto de Cerámica y Vidrio, Consejo Superior de Investigaciones Científicas, 28049 Madrid, Spain*

Abstract: Positron annihilation spectroscopy (PAS), indentation, nanoindentation experiments and scanning electron microscopy (SEM) obser vations were performed on Al_2O_3 ZrO_2 laminates samples to assess the effect of residual stresses on their mechanical and microstructural properties. Layered samples were implemented by slip casting, constituted by two thin Al_2O_3 external layers and an intermediate thick one, consisting of a mixture of Al_2O_3 and monoclinic ZrO_2 in the range 0 30 vol.%. In these systems residual tensile stresses fields were generated inside the external layers during cooling from the sintering temperature, by the expansion of the adjacent ZrO_2 containing layer. SEM observations showed the microstructural effects due to the level of tension related to the zirconia content. A correlation between the PAS parameters and the microstructural changes caused by the presence of residual stresses was found. Nanoindentation measurements were used to trace the sign and magnitude of the residual stress gradient across the interface between the layers.

Keywords: Residual stresses; Ceramics; Multilayers; Positron annihilation; Nanoindentation

1. Introduction

Residual stresses play an important role in many technological applications. In layered ceramics, the presence of compressive residual stresses can delay the propagation of cracks and increase all the associated properties such as hardness, fracture toughness and reliability [1]. The effect of compressive stresses affects not only running cracks, but also the fracture strength by the mechanism of surface strengthening [2,3]. However, the presence of tensile residual stresses usually promotes crack advance through the mate-rial and, consequently, reduces the mechanical response. Furthermore, tensile stresses sufficiently strong can break the material [4]. If there is a metallic phase present in the composition, residual stresses can cause its plastic deformation. Hence, the control of the magnitude of residual stresses in the design and processing of layered ceramic components is an important task [5,6].

Laminar ceramics are a suitable system for generating different levels and distribution of residual stresses. The combination of materials with different coefficients of thermal expansion (CTE, or α) leads to a distribution of compressive and tensile stresses in the layers of the different materials. The magnitude and sign of the stress in each layer depend on the precise selection of the material, and on the structure design and thickness of the layers. After cooling, the layers of the laminate with the higher CTE (α) remain under tensile stress, while those with the lower expansion coefficient remain under compression.

One of the most used laminated systems is Al_2O_3 ZrO_2 (stabilized or not stabilized ZrO_2). This system is very

* Corresponding author. Tel.: +34 916249478; fax: +34 916248749.
E mail address: pparente@fis.uc3m.es (P. Parente).

versatile, since composite layers containing different amounts of these oxides can be combined to give rise to the desired signs and levels of residual stresses. When Y_2O_3-stabilized ZrO_2 is used, it is found that $\alpha(Al_2O_3) < \alpha(t\text{-}ZrO_2)$, but if the zirconia is not stabilized, $\alpha(Al_2O_3) > \alpha(m\text{-}ZrO_2)$ because of the expansion associated with the tetragonal to monoclinic transformation. When this transformation has been employed in alumina zirconia laminates, alumina layers are under tensile stress, while zirconia-containing layers are under compression [7,8]. The expansion of the zirconia-containing layers, and consequently the residual stresses, is controlled by changing the amount of zirconia in the layers [9,10].

Residual stresses can be evaluated by classical elastic theory or the finite element method (FEM) [11,12], employing the data of monolithic samples with the composition of the layers. But these methods do not correspond to the real final residual stresses, as some data can be missed in the initial considerations (porosity, lack of adhesion, etc.). Some methods have been developed to perform direct measurements of the residual stresses. Indentation is the most extended mechanical method for direct determination on coatings and multilayers of both traditional and advanced ceramics and glasses, owing to the simplicity and ease of this test [13 15]. Its unreliability is due to the difficulty of measuring the effects of the combination of the residual stresses generated, and of precisely quantifying the residual surface stresses [16].

Piezo-spectroscopic methods based on the analysis of photo-stimulated fluorescence or Raman bands [17,18] are also largely employed, but these techniques use a probe of only ~10 μm diameter with a penetration depth ~5 μm from the surface [19], so they are applied to local stress measurements [20]. Diffraction techniques have also been employed to determine the magnitude of the residual stresses of ceramics, giving low angle X-ray diffraction clear information about the residual stresses on the surface [21]. In contrast, the neutron diffraction technique per-forms measurements inside the material, but neutrons sources are not easy to achieve or to handle [21,22].

Positron annihilation spectroscopy (PAS) is a non-destructive analytical technique used to study the presence of defects in a material and their nature [23]. It gives information on a relatively thick region down to ~100 μm from the surface, related to the mean positron penetration depth in the sample [23]. In particular, the positron annihilation lifetime spectroscopy (PALS) technique is sensitive to electron density at the defect, and the coincidence Doppler broadening (CDB) technique to the momentum distribution of the electron annihilating with a positron. The combination of these two techniques provides information about the nature of the defects where the positron annihilates, and their surrounding ions.

In the present work, PAS techniques were used to characterize the microstructural features and residual stresses of alumina external layers of symmetrical three-layer Al_2O_3 m-ZrO_2 laminates. Nanoindentation measurements were performed in a cross section of the laminates in order to demonstrate the effect of residual stresses at the interface of the layers.

The combined results of PALS, CDB, indentation and nanoindentation measurements allowed the effect of residual stresses induced during sintering to be established.

2. Experimental procedure

Symmetrical laminates were prepared by sequential slip casting, a versatile forming technique already used to fabricate similar structures [24 27]. The layered structure consisted of a central layer of Al_2O_3 with different amounts of ZrO_2 and ~4000 μm thick, sandwiched between two layers of Al_2O_3 ~400 μm thick; Fig. 1 shows a micrograph of the three-layered structure. The thickness of the external layers was designed large enough to ensure the complete annihilation of the positrons in the alumina layers to be investigated, avoiding any significant contribution of the interface and of the inner layer. The layered samples were named A A$(MZ)_{X\text{vol.}\%}$, where X, the amount of zirconia, was 5, 10, 15, 20 or 30.

α-Al_2O_3 powder with an average grain size of 0.25 μm (Condea HPA 0.5, USA), and monoclinic ZrO_2 powder with an average grain size of 0.3 μm (TZ-O TOSOH, Japan) were used as raw ceramic materials. Both powders were characterized by a purity of 99.9 wt.%.

Suspensions containing 38 vol.% of solid in deionized water and 0.8 wt.% of an acrylic-based polyelectrolyte (Duramax D-3005, Rohm & Haas, USA) as dispersant, were prepared by ultrasonic dispersion and magnetic stirring. Plates 70 × 70 mm^2 were obtained by slip casting on a plaster mold. An Al_2O_3 monolith and five laminates with the internal layer having the different compositions previously indicated were prepared. The thickness of the layers was controlled from the measurement of the wall thickness as a function of the casting time for each suspension, according to previously established kinetics [9].

The green bodies were pre-sintered at 900 °C for 1 h, cut into square samples ~10 × 10 mm^2, and then sintered at 1500 °C for 2 h, with a thermal cycle of 5 °C min^{-1} for the heating and cooling steps. The density of the sintered samples, measured by both the Archimedes and the helium pycnometry method was found to be ~98% theoretical density.

The crystal phases present in the sintered samples were determined by X-ray diffraction analysis, carried out in a

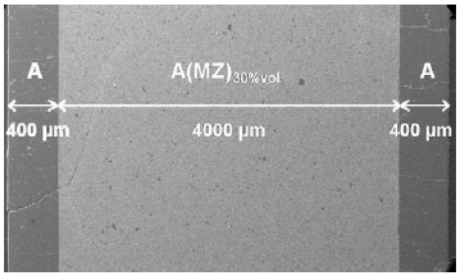

Fig. 1. Micrograph of the three layered structure.

Philips PW 3830 NL diffractometer using Cu $K\alpha_{1,2}$ radiation. X-ray patterns revealed that only α-Al_2O_3 and m-ZrO_2 were present.

The microstructure of the sintered samples was observed by both light microscopy (Carl Zeiss H-P1, Germany) and scanning electron microscopy (SEM) (Zeiss DSM-950, Germany) on polished and thermally etched surfaces. Because the sintered samples presented rounded and equiaxed grains, the diameter of the circle with the same area of grain was used as the characteristic grain size D. The median of the grain size distribution curves was calculated analyzing, for each laminate, a minimum of 750 grains for each phase.

Microhardness measurements were performed at room temperature, applying a load of 49 N with a semi-automatic Vickers hardness tester (Zwick 3212, Germany). The Vickers indentation fracture (VIF) resistance was eval-uated by the Anstis et al. equation as a measurement of the crack growth resistance [28]. Nanoindentation experiments were conducted with a Nanoindenter IIs (MTS Systems, USA), using a Berkovich indenter. The tests were per-formed at room temperature, using the continuous stiffness measurement technique [29,30]. Series of 12 indentations, with an interval of 25 μm between each one, were performed on the cross sections of the layered samples along a direction perpendicular to the interface between the alumina and alumina zirconia layers, in areas free of cracks. The indentation position was measured as a function of the distance to the interface (d), in such a way that it has a negative value for indentations in the Al_2O_3 layer, and it is positive in the central composite Al_2O_3 ZrO_2 layer. The maximum applied load was 700 mN.

PALS and CDB techniques were applied in order to reveal the nature and concentration variations of the microstructural defects present in the alumina external layers. Positron annihilation measurements were performed at room temperature using a ^{22}Na positron source of ~10 μCi sealed between two kapton foils (10 μm thick). For each measurement, the positron source was sandwiched between the outer Al_2O_3 surfaces of two like laminates.

Positron lifetime spectroscopy measurements were performed with a conventional fast fast coincidence spectrometer equipped with two NE111 plastic scintillators placed face to face and each in contact with the pair of samples enclosing the ^{22}Na positron source. The pulses from the detectors that correspond to positron emission and annihilation signals were used as the start and stop of a time to amplitude converter (TAC), which measures the time interval between the two signals and generates a pulse of intensity proportional to the interval and then to the positron lifetime. The corresponding digital pulses were analyzed by a multichannel analyzer (MCA), which displayed them in a graph representing the channels corresponding to fixed time intervals on the x axis, and the number of annihilation events corresponding to the channels on the y axis. The cumulative spectra had $>1 \times 10^6$ counts. The time resolution of the system, measured for ^{22}Na energy settings was 240 ps (full width at half maximum).

The CDB spectra were recorded using two HP Ge detectors in timing coincidence, placed face to face and separated 40 cm from each other. The pair of samples, enclosing a ^{22}Na positron source, were positioned just at the half-way point between the detectors. The pulses from each detector were connected to an ORTEC-572 amplifier with a shaping time of 2 μs. The gain of each amplifier was adjusted to have exactly the same calibration factor for both detectors (81.1 eV channel ^{1}). Signals from the amplifiers were fed into a two-dimensional multichannel analyzer (2D-MCA). Two analogue digital converters were used with a conversion range of 16 K, and the 2D-MCA was adjusted to focus the peak of 511 keV at the center of a 512×512 matrix. The CDB curves analyzed were cumulative spectra formed by addition of 20 spectra that did not exhibit electronic drift, each with $>10^6$ counts in the 512×512 coincidence matrix. The cumulative spectra had $\sim 10^7$ counts in the strip centered on the matrix diagonal that fulfilled the condition $2m_0c^2 - 1.6\ \text{keV} < E_1 + E_2 < 2m_0c^2 + 1.6\ \text{keV}$; where E_1 and E_2 denote the energy of the annihilating gamma-ray pairs, m_0 is the electron rest mass, and c is the light speed. To accentuate the difference between the CDB spectra, and to visualize the defect effect on the intensity of the peaks, the spectra were normalized, dividing the counts at a given γ energy by that corresponding to the pure Al sample. Previously, the areas under the CDB spectra were normalized to unity and smoothed.

3. Results and discussion

3.1. Microstructural characterization

The SEM observation of the sintered monolithic alumina compacts shows a fine and homogeneous microstructure, with an average grain size ~2.5 μm (see Fig. 2a). In layered samples, ZrO_2 grains appear homogeneously distributed among larger Al_2O_3 grains, as the SEM micrograph of the $A(MZ)_{15vol.\%}$ intermediate layer shows (Fig. 2b). The measured average sizes of Al_2O_3 and ZrO_2 grains for each laminate are shown in Table 1. For all the layered materials, the outer α-Al_2O_3 layers present a larger grain size of 2.4 μm, similar to that in the alumina monolith. The presence of zirconia inhibits alumina grain coarsening. As a result, the dimension of the alumina grains decreases in the central layer. Additionally, the pres-ence of ZrO_2 promotes densification, reducing the porosity [31].

SEM images of polished and thermally attached sections of the A $A(MZ)_{X vol.\%}$ samples show a well-defined interface between the layers. Laminates prepared with a ZrO_2 content in the central layer <20 vol.% do not show signs of delamination (see Fig. 3a). With a greater amount of zirconia, evident delamination phenomena occur, as shown in Fig. 3b.

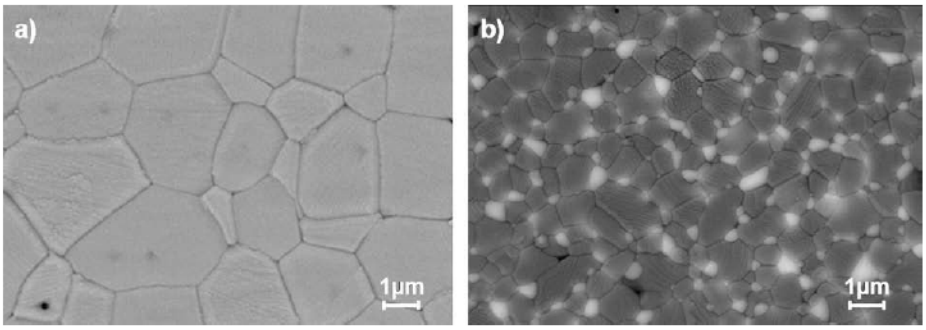

Fig. 2. SEM BE micrographs of: (a) the cross section of the Al_2O_3 monolithic and (b) the central layer of sample A A$(MZ)_{15vol.\%}$. Zirconia grains (white) appear to be well homogeneously distributed among the alumina grains (gray).

Table 1
Grain size of Al_2O_3 and ZrO_2 grains in the central layers of the laminates.

D_{50} (μm)	m ZrO_2 content (vol.%)				
	5	10	15	20	30
ZrO_2	0.24	0.28	0.30	0.30	0.40
Al_2O_3	0.94	0.70	0.74	0.57	0.61

The delamination phenomenon for this class of laminates arises from the release of residual stresses at the layer interfaces due to the tetragonal to monoclinic transformation of the ZrO_2 in the central layer during the cooling of the sintering step. This phase transformation causes a vol-ume expansion of ~4%, which results in biaxial compres-sive stresses produced in the central A A$(MZ)_{Xvol.\%}$layer, while tensile stresses are generated in the external Al_2O_3 layer. The level of these stresses depends on the thickness, elastic constant and compressive strain of each layer [7,10,32]. Using the data reported in the literature and the classical residual stress equation [9,10], the residual tensile stresses inside the alumina outer layers were evalu-ated as 850, 550, 300 and 30 MPa for samples with 30, 20, 10 and 5 vol.% MZ, respectively. However, the com-pressive stresses for the central layer have been evaluated as −170, −110, −61 and −7 MPa for 30, 20, 10 and 5 vol.% MZ. SEM observations showed that the presence of cracks, induced by residual stresses, is related to the zir-conia content. In particular, for contents of $ZrO_2 \geqslant 10$ vol.%, cracks originating at the alumina surface were

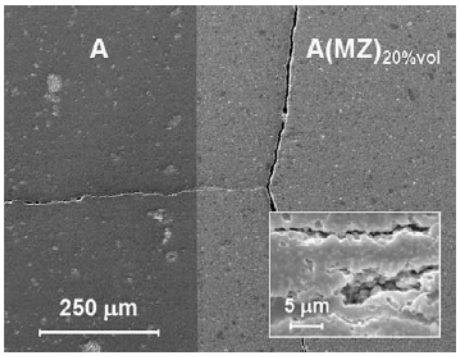

Fig. 4. SEM SE micrograph of the cross section of sample A A$(MZ)_{20vol.\%}$. Showing the propagation and bifurcation of a crack. Detail of the crack in the internal layer.

observed. They propagate through the laminate, enter in the central layer, and bifurcate at a characteristic length, as observed in Fig. 4 for sample A A$(MZ)_{20vol.\%}$. Deeper detail of the fracture reveals that the propagation mode of the crack is essentially intergranular. These observations are in agreement with the development of compressive stresses in the central layer. For ZrO_2 contents <10 vol.%, the tensile stress developed in the surface is not intense enough to generate cracks.

3.2. *Indentation measurements*

Table 2 reports the Vickers hardness, HV, and the VIF resistance, for the alumina monolith and for the central

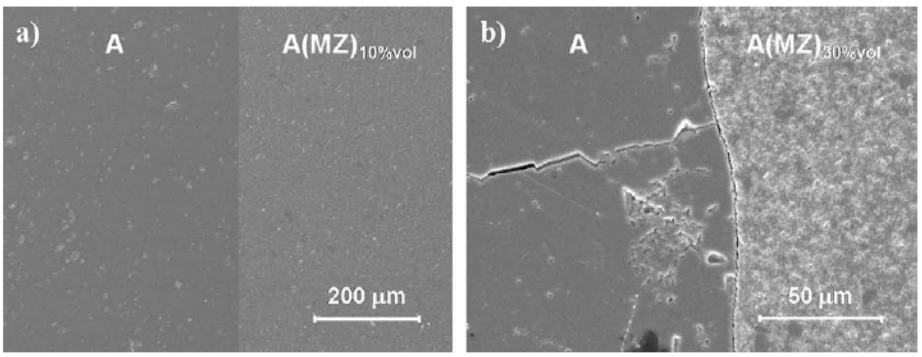

Fig. 3. SEM SE micrographs of the cross sections showing: (a) the good adherence between the layers of sample A A$(MZ)_{10vol.\%}$ and (b) a partial delamination at the interface between the alumina and alumina zirconia layers of sample A A$(MZ)_{30vol.\%}$.

layer of each laminate sample. The hardness value decreases with increasing ZrO_2 content, while the VIF resistance or crack growth resistance value increases with ZrO_2 content. This inverse relationship between hardness and crack growth resistance was found previously [33]. The hardness value obeys a linear mixture law, since the hardness of pure zirconia is lower than the alumina hard-ness. The low value of the hardness of the alumina mono-lith compared with the A $A(MZ)_{5vol.\%}$ value is due to the fact that the alumina grain size in the alumina monolith is twice the alumina size in the composite layer, and the hardness is inversely correlated with the grain size [34]. The enhancement of the crack growth resistance of the composite with increasing zirconia is mostly attributed to the tetragonal to monoclinic transformation, which occurs with a zirconia volume expansion that leads to the forma-tion of grain boundary microcracks, which interact with the propagating crack tip to lower the tensile stress in the crack and inhibit crack growth [35,36]. In addition, the crack growth resistance increases with the amount of zirco-nia, owing to the higher compressive stress intensity gener-ated by a larger thermal expansion coefficient mismatch between the pure alumina layer and the mixture layer. For $X < 20$, the fracture toughness of the alumina monolith is higher than that corresponding to the composite. This behavior is also due to the greater size of the alumina grain in the monolith. Nevertheless, it is convenient to remark that crack growth resistance values may be overestimated because the VIF test generates a complex crack system with substantial deformation residual stresses around the cracks that is difficult to describe and quantify.

3.3. Nanoindentation measurements

Fig. 5a and b shows the load penetration depth curves for selected nanoindentations performed on the cross-sectional area of the Al_2O_3 layers for the two laminate samples A $A(MZ)_{5vol.\%}$ and A $A(MZ)_{20vol.\%}$, respectively. The curves evidence the effect of the residual stresses on the indentation load displacement behavior. At a given indentation depth, the indentation load for the compressive stressed areas is higher than that for the unstressed area, but the load for the tensile stressed areas is lower [11,37]. For the laminate sample A $A(MZ)_{20vol.\%}$, the effect of residual stress in the Al_2O_3 layer is evident, changing the type of residual stress from compressive to tensile, depend-ing on the distance to the interface. The residual stresses generated in the laminate sample A $A(MZ)_{5vol.\%}$ are not enough to observe any effect. Fig. 6 shows the load pene-

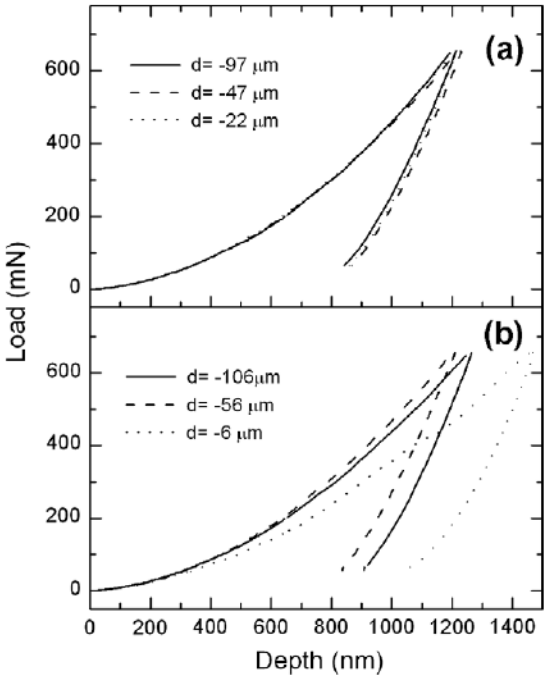

Fig. 5. Nanoindentation load penetration curves for selected indentations in the Al_2O_3 layers of (a) sample A $A(MZ)_{5vol.\%}$ and (b) sample A $A(MZ)_{20vol.\%}$. The term d denotes the distance from the interface.

tration depth curves as a function of the distance to the interface (d) in the central layer of the laminate samples A $A(MZ)_{20vol.\%}$. Far away from the interface, i.e., d 143 μm, the behavior matches that corresponding to a stress-free area. Moving towards the interface, the observed behavior is compatible with areas with more and more compressive residual stresses. This trend changes for a short distance from the interface, in this case d 18 μm, where the load penetration depth curve is consistent with a region with lower residual stresses.

The effect of residual stresses on the hardness value is a question extensively discussed. It was found that hardness decreases with internal tensile stresses and increases with internal compressive stresses [11]. Several theoretical approaches for elucidating the dependence of the nanohardness on the residual stresses were proposed [37 40], some of them revealing the important role of pile-up or sink-in deformations around the indentation in the deter-mination of the nanohardness values.

In Fig. 7, the nanohardness values determined at a contact depth of 800 nm through the alumina/alumina zirconia interface of the cross-sectional area of the laminate are reported. At distances far away from the interface,

Table 2
Vickers hardness (HV) and VIF resistance, measured in the middle of the central layer of the samples.

	m ZrO_2 content (vol.%)					
	0	5	10	15	20	30
HV (GPa)	15.6 ± 0.5	15.7 ± 0.4	14.5 ± 0.6	14.8 ± 0.5	13.8 ± 0.4	10.9 ± 0.5
VIF resistance (MPa $\sqrt{m}$)	4.6 ± 1.3	3.3 ± 0.2	3.8 ± 0.2	3.1 ± 0.2	4.9 ± 0.3	5.8 ± 0.5

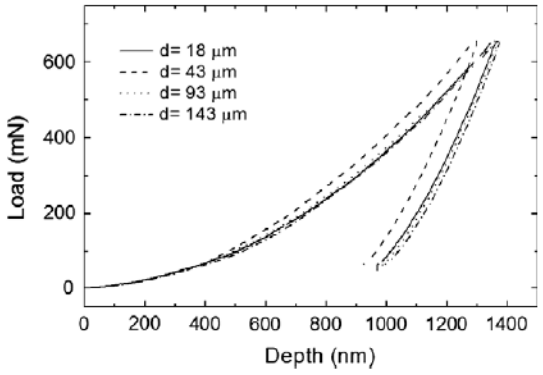

Fig. 6. Nanoindentation load penetration curves performed in the central layer of sample A $A(MZ)_{20vol.\%}$, at the distance d from the interface.

the nanohardness value of the Al_2O_3 ZrO_2 layer agrees with the value for corresponding composition: the hardness value decreases as the ZrO_2 content increases. The behavior of the nanohardness near the interface is compatible with the load penetration curves, which is related to the type and magnitude of the internal residual stresses in the laminates: compressive in the central $A(MZ)_{X vol.\%}$ layer, and tensile in the outer Al_2O_3 layer. Microscopic distributions of residual stresses in multilayered systems have been evaluated by Raman and fluorescence piezo-spectroscopy, and a parabolic stress profile near the interface between layers has been found [18]. This could be the reason for the nanohardness behavior observed close to the interface.

For a system composed of n layers of composition A and thickness t_A, and $(n - 1)$ layers of composition B and thickness t_B, the biaxial residual stress inside one layer is related to the stress inside the adjacent one by [9]:

$$\sigma_B = -\sigma_A \frac{n t_A}{(n-1) t_B} \quad (1)$$

In the present work n 2, A corresponds to Al_2O_3 with t_A 400 μm, and B is $A(MZ)_{X vol.\%}$ with t_B 4000 μm. Therefore, $\sigma(A(MZ)_{X vol.\%})$ $-0.2\ \sigma(Al_2O_3)$, i.e., the magnitude of compressive stresses in the internal layer of each laminate is lower than the magnitude of tensile stresses in the external layer. This relation should be taken as a good estimation of the stress relation between adjacent layers at the surface of the laminates. According to this result, and taking into account that the effect of compressive stresses in nanohardness values is smaller than that of the tensile stresses [11], the dependence of the residual stresses on the nanohardness values should be stronger in the Al_2O_3 layer than in the composite layer, as the experimental measurements confirmed (see Fig. 7).

3.4. Positron measurements

In order to determine the nature of defects induced by the presence of residual stresses, positron lifetime measurements (PALS) were carried out in the external Al_2O_3 surface layers of the whole set of sintered laminates and of the monolith alumina sample.

As the characteristic lifetimes of intrinsic and microstructural defects induced in such materials are very similar [41], all positron lifetime spectra were properly fit to only one component. The average lifetime was then taken as a statistically accurate parameter, adequate to monitor changes in the lifetime spectra, as indicated by the small value of χ^2 (always <1.2) obtained when analyzing the lifetime spectra with the POSITRONFIT program [42].

In Fig. 8, the average positron lifetime measured for samples A $A(MZ)_{X vol.\%}$ as a function of zirconia content in the central layer was reported. The mean positron lifetime for a single crystal of high purity Al_2O_3 was also measured as a reference; its value, equal to 161 ± 1 ps, is in good agreement with the reported values [43]. This lifetime value would be an unequivocal signature for positron annihilation in the bulk of Al_2O_3. The mean positron lifetime measured for the monolithic Al_2O_3 sample is τ^- 170 ± 2 ps. Fig. 8 shows that the addition of ZrO_2 in the central layer results in the increase in the average positron lifetime, which value scales with the presence of defects in the sin-tered material. Indeed, for the laminate with the highest zirconia content, i.e., X 30, τ^- reaches a value of 190 ± 2 ps. This increase is linked to the reduction in the electron density [23] due to both the deformation of the

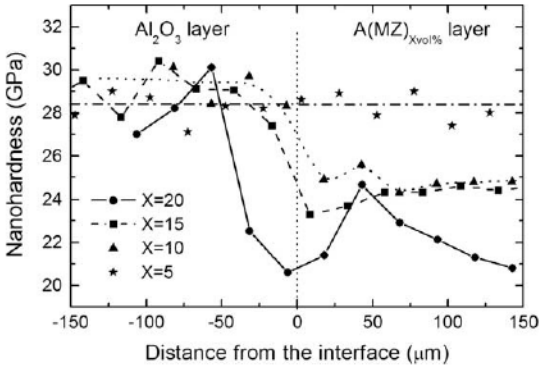

Fig. 7. Nanohardness values at a contact depth of 800 nm across the cross sections of the laminates studied.

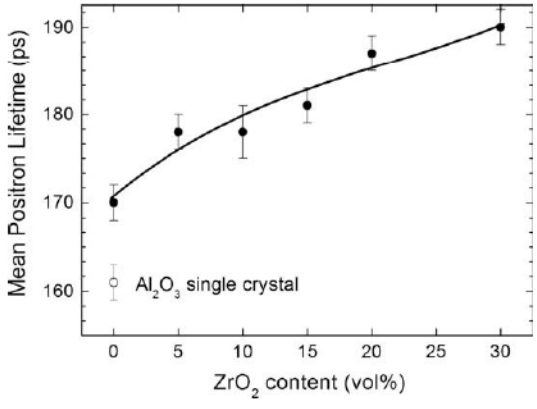

Fig. 8. Mean positron lifetime as a function of the ZrO_2 content in the central layer.

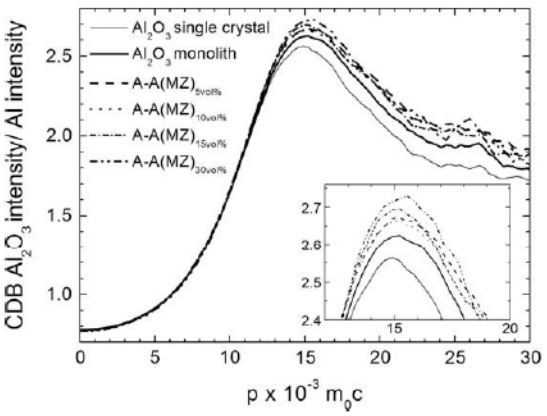

Fig. 9. CDB ratio spectra for the whole A $A(MZ)_{X\text{vol.\%}}$ series. The detail of the peak points out variations in the intensity.

crystal lattice associated with the most intense state of tension to which the alumina layer is subjected, and the positron trapping in structural defects. All τ^{-} values are higher compared with those reported in other studies on Al_2O_3 single crystal vacancies [44,45]. For these materials, there-fore, besides positron trapping in aluminum monovacan-cies V_{Al}, trapping in more complex defects such as bivacancies (V_{Al} V_{Al}), (V_O V_{Al}) or complex vacancies impurities also occurs, all contributing to the increase in average lifetime. No lifetime components associated with other cavities and defects were found.

CDB measurements were performed to obtain information about the ions surrounding the positron trapping sites in the Al_2O_3 layers for each sample of the laminates set (Fig. 9). In the same figure, the CDB ratio spectra of the Al_2O_3 monolith and of an Al_2O_3 single crystal, considered as a reference, are also reported. All spectra show a peak centered at $\sim 14.8 \times 10^{-3} m_0c$, which is characteristic of positron annihilations with the valence electrons of O^{2} ions. It can be observed that, in the low-momentum region, no meaningful differences among the different CDB ratio spectra exist, and their intensity is <1. The peak intensity slightly increases with the ZrO_2 content in the central layer, and remains above the corresponding value for the Al_2O_3 single crystal.

These CDB results, and the corresponding increase in the mean positron lifetime from 170 to 190 ps with an increasing amount of zirconia, unambiguously indicate an increase in concentration of structural defects associated with O^{2} ions. They cannot be attributed to positron annihilation in either anionic vacancies or anionic vacancy agglomerates, because positron annihilations in these types of defects should induce a strong intensity decrease in the peak centered at $14.8 \times 10^{-3} m_0c$, and a subsequent increase in the intensity in the low-momentum region ($p \approx 0$), compared with the intensity of the spectrum of Al_2O_3 single crystal [46]. Also these results cannot be attributed to positron annihilation in vacancy clusters, because the lifetime spectra would present a large compo-nent of 300 400 ps, typical of this type of defects [44], which was not observed. Thus, the results obtained can be attributed to positron annihilation in cationic vacancies or at dislocations induced by the residual stress generated by the phase transformation of the unstabilized zirconia [43].

4. Conclusions

Al_2O_3 ZrO_2 laminates with ZrO_2 content ranging from 0 to 30 vol.% were produced by slip casting. Compressive stresses were generated in the central $A(MZ)_{X\text{vol.\%}}$ layer, whereas tensile stresses appeared in the outer layer.

Nanoindentation measurements performed across the interface demonstrated the effect of residual stress gradient on the load displacement curves and nanohardness. PALS and CDB techniques provided information concerning the effect of residual stresses at a microstructural level. Correlation was found between the increase in the positron mean lifetime values and intensity of Doppler peaks with zirconia content. The results obtained were attributed to positron annihilation in cationic vacancies and dislocations associated with O^{2} ions, induced by residual stresses. The reliability of changes in spectroscopic parameters related to residual stresses was confirmed by the results of the SEM observations and nanoindentation measurements.

Acknowledgements

This work was supported by Spanish Government under Contract MAT2006-01038. The authors gratefully acknowledge the financial support from the Comunidad de Madrid and the Ministry of Education and Science of Spain, through the ESTRUMAT-CM (MAT/77) programs. P. Parente thanks the Comunidad de Madrid for her PIA appointment and the Dr. Gianclaudio Ferro for the guidance during her stay at ENEA Bologna Research Centre.

References

[1] Rao MP, Sanchez Herencia AJ, Beltz GE, McMeeking RM, Lange FF. Science 1999;286:102.
[2] Gurauskis J, Sanchez Herencia AJ, Baudin C. J Eur Ceram Soc 2007;27:1389.
[3] Lin GY, Virkar AV. J Am Ceram Soc 2001;84:1321.
[4] Hillman C, Suo ZG, Lange FF. J Am Ceram Soc 1996;79:2127.
[5] Chan HM. Ann Rev Mater Sci 1997;27:249.
[6] Sánchez Herencia AJ, Baudín C. Bol Soc Esp Ceram V 2009;48:223.
[7] Bermejo R, Pascual J, Lube T, Danzer R. J Eur Ceram Soc 2008;28:1575.
[8] Virkar AV, Huang JL, Cutler RA. J Am Ceram Soc 1987;70:164.
[9] Bermejo R, Baudin C, Moreno R, Llanes L, Sanchez Herencia AJ. Compos Sci Technol 2007;67:1930.
[10] Pontin MG, Rao MP, Sanchez Herencia AJ, Lange FF. J Am Ceram Soc 2002;85:3041.
[11] Zhao MH, Chen X, Yan J, Karlsson AM. Acta Mater 2006;54:2823.
[12] Huber N, Heerens J. Acta Mater 2008;56:6205.
[13] Buchheit TE, Tandon R. J Mater Res 2007;22:2875.
[14] Moon H, Bahk JH, Lange FF. Int J Mater Res 2007;98:674.
[15] Yeh CH, Hon MH. J Mater Sci 2000;35:1037.

[16] Quinn GD, Bradt RC. J Am Ceram Soc 2007;90:673.
[17] Zhao X, Xiao P. Surf Coat Technol 2006;201:1124.
[18] de Portu G, Micele L, Sekiguchi Y, Pezzotti G. Acta Mater 2005;53:1511.
[19] Diniz AV, Ferreira NG, Corat EJ, Trava Airoldi VJ. Diam Relat Mat 2004;13:526.
[20] Tanaka M, Kitazawa R, Tomimatsu T, Liu YF, Kagawa Y. Surf Coat Technol 2009;204:657.
[21] Kesler O, Matejicek J, Sampath S, Suresh S, Gnaeupel Herold T, Brand PC, et al. Mater Sci Eng A Struct 1998;257:215.
[22] Ruiz Hervias J, Bruno G, Gurauskis J, Sanchez Herencia AJ, Baudin C. Scripta Mater 2006;54:1133.
[23] Krause Rehberg R, Leipner H. Positron annihilation in semiconduc tors: defect studies. Berlin: Springer; 1999.
[24] Bermejo R, Sanchez Herencia AJ, Baudin C, Llanes L. Bol Soc Esp Ceram V 2006;45:352.
[25] Orlovskaya NA, Kuebler J, Subotin VI, Lugovy M. Advanced fibers, plastics, laminates and composites. In: Materials research society symposium proceedings 2002;702:325.
[26] Sglavo VM, Paternoster M, Bertoldi M. J Am Ceram Soc 2005;88:2826.
[27] Bermejo R, Torres Y, Sanchez Herencia AJ, Baudin C, Anglada M, Llanes L. Acta Mater 2006;54:4745.
[28] Ponton CB, Rawlings RD. Mater Sci Technol 1989;5:865.
[29] Pethica JB, Oliver WC. Mechanical properties of nanometer volumes of materials: use of the elastic response of small area indentations. In: Proceedings of the materials research society symposium on thin films: stresses and mechanical properties, Pittsburgh, PA; 1989.
[30] Oliver WC, Pharr GM. J Mater Res 1992;7:1564.
[31] Wang J, Stevens R. J Mater Sci 1989;24:3421.
[32] Lugovy M, Orlovskaya N, Slyunyayev V, Gogotsi G, Kubler J, Sanchez Herencia AJ. Compos Sci Technol 2002;62:819.
[33] Moraes MCC, Elias CN, Duailibi Filho J, Oliveira LG. Mater Res 2004;7:643.
[34] Rice RW, Wu CC, Borchelt F. J Am Ceram Soc 1994;77:2539.
[35] Tomaszewski H. Ceram Int 1988;14:117.
[36] Hori S, Yoshimura M, Somiya S. J Am Ceram Soc 1986;69:169.
[37] Suresh S, Giannakopoulos AE. Acta Mater 1998;46:5755.
[38] Lee YH, Kwon D. Scripta Mater 2003;49:459.
[39] Tsui TY, Oliver WC, Pharr GM. J Mater Sci 1996;11:752.
[40] Bolshakov A, Oliver WC, Pharr GM. J Mater Res 1996;11:760.
[41] Lagerlof KPD, Grimes RW. Acta Mater 1998;46:5689.
[42] Kirkegaard P, Eldrup M. Comput Phys Commun 1972;3:240.
[43] Shek CH, Gu TS, Lin GM, Lai JKL. Appl Phys A Mater 1998;66:413.
[44] Schaefer HE, Forster M. Mater Sci Eng A Struct 1989;109:161.
[45] Forster M, Claudy W, Hermes H, Koch M, Maier K, Major J, et al. Mater Sci Forum 1991;1005:105.
[46] Hasegawa M, Nagashima Y, Kawashima K, Hyodo T, Yamaguchi S, Forster M, et al. Nucl Instrum Meth B 1994;91:263.